2019 SENSOR SIGNAL PROCESSING FOR DEFENCE CONFERENCE(2019 SSPD), Brighton, UK, 9th – 10th May
DOI:10.1109/SSPD.2019.8751653

Numerical Characterisation of Quasi-Orthogonal Piecewise Linear Frequency Modulated Waveforms

Leon Kocjancic[1], Alessio Balleri[1] and Thomas Merlet[2]
[1]Centre for Electronic Warfare, Information and Cyber, Cranfield University,
Defence Academy of the United Kingdom, Shrivenham, SN6 8LA
[2]Thales Optronique SAS, Elancourt, 78995, France

***Abstract*—This paper presents an analysis of the Doppler tolerance and isolation properties of five different sets of piecewise linear frequency modulated (PLFM) waveform triplets consisting of a combination of LFM subchirps. Different combinations of PLFM signals are used to produce waveforms with the same time-bandwidth product and optimise them with respect to isolation. The performance of the proposed waveforms are numerically investigated and a comparison between sets is presented. Results confirm that the waveforms have quasi-orthogonal properties and exhibit a degree of Doppler tolerance.**

I. Introduction

The design of orthogonal waveforms represents one of the major research challenges for multi-channel and multi-function radar systems. Recently, multiple-input multiple-output (MIMO) techniques have been adopted by the radar community as they can provide benefits, such as improved target detection performance, improved angle estimation accuracy and decreased minimum detectable velocity [1]–[4]. MIMO radars can operate in two different ways, namely in statistical and coherent modes of operation. Statistical MIMO radar systems deploy broadly separated antennas, whereas coherent MIMO radars feature closely spaced antennas. In both cases, each antenna element transmits a waveform orthogonal to adjacent waveforms transmitted by all other antenna elements. In addition to common modes of operation, a multi-beam radar (MBR) with collocated antennas can be devised as well. This type of radar uses an orthogonal waveform for each of its beams to form separate radar channels with different properties [5], [6]. A linear combination of orthogonal waveforms is transmitted for each channel. Isolation between channels of an MBR is key and enables multiple simultaneous functionalities requiring a different resource allocation, such as radar altimetry, target tracking, proximity activation, etc.

The most common implementations of orthogonal waveforms, that reduce mutual interference in its entirety, are time division multiplexing (TDM) [3] and frequency division multiplexing (FDM) [7]. Although the aforementioned techniques work well in the domain of telecommunications, they present limitations when used for radar sensing and detection. In the case of TDM, a target may be moving which would affect different time delayed waveforms differently. FDM, on the other hand, could produce different responses for different frequency bands as the target radar cross section (RCS) is also a function of frequency. To counteract both problems, waveforms with the same time and frequency support can be used and their orthogonality is achieved by employing waveform diversity (WD).

This paper focuses on linear frequency modulated (LFM) waveforms as they have good Doppler tolerance and constant amplitude, which allows the transmitting amplifiers to operate in a saturated mode. The pulse compression, low sidelobes and ease of generation are additional advantages of LFM waveforms. Moreover, LFM waveforms do not require any prior knowledge of the target response and that makes them suitable for detection. It has been shown that LFM waveforms present quasi-orthogonal properties when chirp rate diversity is exploited [8], [9]. The orthogonal properties have been analysed and demonstrated in many applications of telecommunications and radar signal processing. In [10] the authors showed how LFM chirps can be used in multiuser communication schemes to form independent channels and reduce mutual interference. Additionally, LFM chirps have been used as pilot signals for channel estimation [10]. Chirp rate diversity can be applied to MIMO synthetic aperture radars (SAR) as well, where a high degree of isolation, large time-bandwidth product and constant signal envelope are required to form orthogonal waveforms [11]. A similar approach was used to investigate piecewise linear frequency modulated (PLFM) waveforms and their use for different types of MIMO radar when Doppler tolerance and no prior knowledge about the target are required [12], [13]. PLFM waveforms consist of multiple time-delayed chirps stacked together so that amplitude of the signal remains constant.

This paper is focused on a numerical characterisation of five proposed sets of PLFM waveforms. Each set is investigated and compared with respect to isolation performance and Doppler tolerance.

II. Waveform Design

A. Signal Model

Let us consider PLFM signals of amplitude A, obtained as the combination of $N = 2$ LFM waveforms, with a complex envelope

$$s_i(t) = A \sum_{n=1}^{N} s_{i,n} \tag{1}$$

© 2019 IEEE. Personal use of this material is permitted. Permission from IEEE must be obtained for all other uses, in any current or future media, including reprinting/republishing this material for advertising or promotional purposes, creating new collective works, for resale or redistribution to servers or lists, or reuse of any copyrighted component of this work in other works.

where

$$s_{i,n} = \text{rect}\left(\frac{t-\tau_{i,n}}{T_{i,n}}\right) e^{2\pi j f_{i,n}(t-\tau_{i,n})} e^{\pi j \mu_{i,n}(t-\tau_{i,n})^2} \quad (2)$$

The frequency offset and chirp rate of the nth subchirp with duration $T_{i,n}$ and bandwidth $B_{i,n}$ are defined as $f_{i,n}$ and $\mu_{i,n} = B_{i,n}/T_{i,n}$, respectively. The bandwidth $B_{i,n}$ is positive for up-chirps and negative for down-chirps and the rectangular function is defined as

$$\text{rect}\left(\frac{t}{T}\right) = \begin{cases} 1, & t \in [0,T] \\ 0, & \text{otherwise} \end{cases} \quad (3)$$

We study the orthogonal properties and Doppler tolerance of five sets of different waveform triplets (that is $i = 1, .., 3$), all of the same energy, with the frequency modulation and design shown in Fig. 1 and with the parameters given in Table I.

B. Characterisation Metrics

The level of interference between a pair of waveforms $s_i(t)$ and $s_j(t)$ in the presence of a target inducing a Doppler shift can be described by the cross-ambiguity function

$$\chi_{i,j}(\tau, f_D) = \int s_i^*(t) s_j(t+\tau) e^{j2\pi f_D t} dt \quad (4)$$

The isolation is defined as the ratio between the peak of the ambiguity function and the cross-ambiguity function as

$$I_{i,j}(\tau, f_D) = \left|\frac{\chi_{i,i}(0,0)}{\chi_{i,j}(\tau, f_D)}\right| = \left|\frac{\chi_{j,j}(0,0)}{\chi_{j,i}(-\tau, f_D)}\right| \quad (5)$$

and the minimum level of isolation is

$$\overline{I}_{i,j} = \frac{\chi_{i,i}(0,0)}{\max_{\tau, f_D} |\chi_{i,j}(\tau, f_D)|} \quad (6)$$

For each waveform triplet, the lowest isolation between all possible pair combinations is taken as a reference and therefore

$$\overline{I}_{set} = \min_{i,j} \overline{I}_{i,j} \quad (7)$$

with $i \in \{1,2,3\}$, $j \in \{1,2,3\}$ and $i \neq j$. The effects of Doppler on orthogonality between waveform pairs is analysed by the zero-delay cut of the cross-ambiguity function

$$\chi_{i,j}(0, f_D) = \int s_i^*(t) s_j(t) e^{j2\pi f_D t} dt \quad (8)$$

and the filter mismatch loss due to the Doppler shift can be determined as

$$M_i(f_D) = \frac{\max_\tau |\chi_{i,i}(\tau, f_D)|}{\chi_{i,i}(0,0)} \quad (9)$$

As a reference, the Doppler performance of s_i within the Doppler interval $f_D \in [f_{D,min}, f_{D,max}]$ is indicated as

$$\overline{M}_i = \min_{f_D} M_i(f_D) \quad (10)$$

Finally, the average power leakage between a pair of waveforms after matched filtering in the interval $\tau \in [\tau_{min}, \tau_{max}]$ is indicated by the peak to average cross-correlation, also known as peak to average power ratio (PAPR), and can be calculated as

$$\overline{P}_{i,j} = (\tau_{max} - \tau_{min}) \frac{\chi_{i,i}(0,0)}{\int_{\tau_{min}}^{\tau_{max}} |\chi_{i,j}(\tau, 0)| d\tau} \quad (11)$$

III. Numerical Simulations

A. General Parameters

In this section, a comparison between the five proposed waveform triplets is presented along with their frequency modulation schemes, time delay cuts, Doppler cuts and isolation figures. The design of the three waveforms forming each triplet is given in the first column of Fig. 1 for the five proposed sets. For clarity, Fig. 1 is indicative and does not take into account the exact design parameters of each waveform given in Table I. All waveforms s_i have the same time duration T and bandwidth B and therefore a constant time-bandwidth product of $BT = 5000$ to ensure a fair comparison of the results. For the simulations presented in this paper, the time duration was fixed to $T = 50\,\mu\text{s}$, the bandwidth to $B = 100\,\text{MHz}$ and the sampling frequency was $f_s = 400\,\text{MHz}$. The maximum Doppler shift considered was $f_{D,max} = 160\,\text{kHz}$ which is sufficient to account for targets travelling at Mach 2 for a carrier frequency of $35\,\text{GHz}$. All pair combinations in each of the five sets are characterised by the isolation performance $\overline{I}_{i,j}$, Doppler tolerance $\overline{M}_i$ and PAPR $\overline{P}_{i,j}$. For each set the worst case figure of the isolation $\overline{I}_{set}$ is given as well.

B. Comments on the Results

Set 1 consists of an up-chirp, a down-chirp and a combination of up and down chirps. Table I shows that the up-chirp and the down-chirp are the combination pair with the best isolation performance. This is in agreement with the results obtained in [5] that showed the isolation improves with the time-bandwidth product as

$$\overline{I}_{i,j} \approx \sqrt{BT}, BT >> 1 \quad (12)$$

Furthermore, for chirps with the same duration and different chirp rates, a lower bound on the isolation has been found as [5]

$$\overline{I}_{i,j} > \sqrt{\frac{|\Delta B| T}{2}} \quad (13)$$

Note that Eq. 13 depends on the bandwidth difference between two waveforms with the bandwidth defined as a signed value (i.e. positive for an up-chirp and negative for a down-chirp). As a result, chirp pairs with opposite frequency rates exhibit higher isolation values than chirp pairs with only increasing or decreasing rates. The cross-correlation values shown in Fig. 1(b) corroborate that up and down-chirps (s_1, s_2) have lower value of interference in comparison to the case with two up-chirps $(s_1, s_{3,1})$. In this case, splitting s_3 into two subsignals provides chirp rate diversity and results in better orthogonality. The highest value of the cross-correlations $\chi_{3,2}(\tau, 0)$ and $\chi_{1,3}(\tau, 0)$ occurs for negative delays and is due to the contribution of two intersection points in the time-frequency space (see Fig. 1(a)). According to Eq. (13), the intersection of the two up-chirps ($s_{3,1}$ and s_1) contributes more energy than the other intersection ($s_{3,2}$ and s_1) that consists of up- and down-chirp.

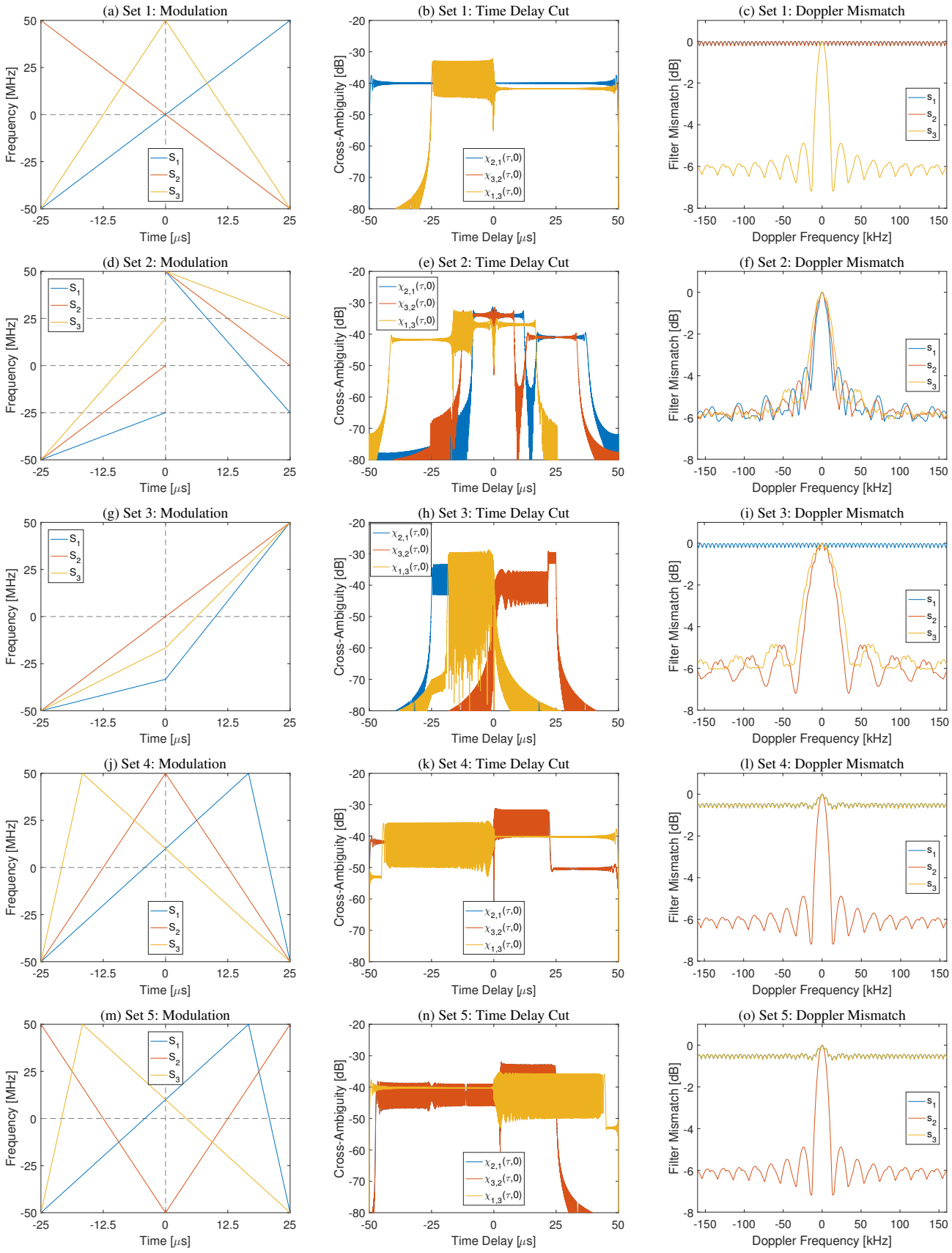


Fig. 1. First column depicts frequency modulations, second column shows zero Doppler cuts of normalised cross-ambiguity functions $\chi_{i,j}(\tau, 0)$ and third one filter mismatch losses due to Doppler shift $M_i(f_D)$.

Set 2 consists of waveforms made of disjoint subchirps and was introduced in [12]. The time duration of each subchirp was selected via an optimisation iteration aimed at minimising isolation. Table I shows the best isolation occurs when the first subchirp has a time duration of $T/2 - \Delta T$ and $\Delta T = -0.425\,\mu s$. The best isolation values are obtained when subchirps occupy approximately half of the waveform duration. This can be seen in Fig. 2 showing the value of isolation as a function of ΔT. Decreasing time duration of a chirp effectively decreases the isolation and optimal isolation values occur when the minimal time duration is maximised. Fig. 1(e) shows that the cross-correlations $\chi_{2,1}(\tau, 0)$ and $\chi_{3,2}(\tau, 0)$ have the highest value in the centre, where single intersections in the time-frequency modulation plots contribute the most. The aforementioned intersections correspond to the pairs of up-chirps ($s_{1,1}, s_{2,1}$ at positive delays) and down-chirps ($s_{1,2}, s_{2,2}$ at negative delays) both of which have the same $|\Delta B|T$ and therefore comparable level of isolation. Similar reasoning holds for $\chi_{3,2}(\tau, 0)$.

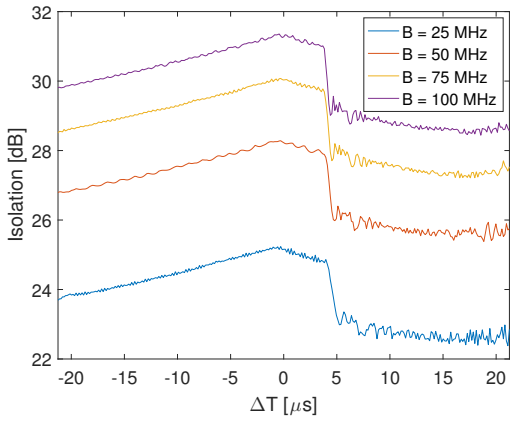


Fig. 2. Optimisation results for set 2 with parametrised bandwidths. Isolation obtains higher values when time duration of all subsignals is comparable.

Set 3 was previously used for time-synchronised multi-channel communications systems [10], hence its isolation values are worse when the waveforms are transmitted with different time delays. The waveforms were defined according to the frequency modulations shown in Fig. 1(g). Optimisation results were obtained for a fixed s_2 and by varying the other two waveforms so to change the starting frequencies $f_{1,2}$ and $f_{3,2}$ whilst adjusting the bandwidths $B_{1,1}$, $B_{3,1}$ accordingly. Fig. 3 shows that isolation increases when the intermediate frequencies have opposite signs and that the plot is symmetric around the axis $f_{1,2} = f_{3,2}$. Results indicate two optimal solutions and one of them is defined in Table I. It shows that the first subchirp $s_{2,1}$ has a constant frequency value. This confirms the results in Fig. 3 as the optimal solutions are located at the edges of the frequency distribution. The optimisation variables were bounded within the interval $f_{1,2}, f_{3,2} \in [-50\,\text{MHz}, 50\,\text{MHz}]$.

Sets 4 and 5 were obtained by fixing s_2 and optimising s_1 and s_3. The bandwidth of each subchirp was fixed whilst

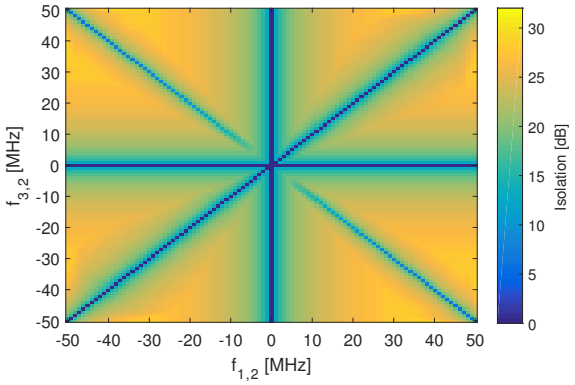


Fig. 3. Optimisation results for the waveform set 3. Isolation of the the entire set is shown as a function of optimisation parameters $f_{1,2}$ and $f_{3,2}$.

the time duration was varied according to $T_{i,1} = T/2 + \Delta T_i$. In this case, the optimisation variables were bounded within the intervals $\Delta T_1, \Delta T_3 \in [-22.5\,\mu s, 22.5\,\mu s]$. Fig. 4 and Fig. 5 show that the optimal regions are those where ΔT_1 and ΔT_3 have opposite signs with the optimal values being in the corners. In the case of set 4, the highest values of cross-ambiguity function $\chi_{3,2}(\tau, 0)$ (Fig. 1(k)) are a contribution of intersections of chirp pairs $s_{s_2,1}, s_{3,1}$ and $s_{s_2,2}, s_{3,2}$ for positive delays. This contribution can be minimised by employing chirp rate diversity and therefore increasing the chirp rate difference between corresponding pairs. The difference is maximised by increasing the values of $|\Delta T_3|$ which leads to the optimal figures noted in Table I and shown in Fig. 4. Similar reasoning is suitable for set 5. The difference in this case is that the chirp pairs $s_{2,1}, s_{3,1}$ and $s_{2,2}, s_{3,2}$, contributing to the maximum value of $\chi_{3,2}(\tau, 0)$ for positive delays, have opposite slopes. This improves isolation performance as shown in Fig. 5 and corroborates Eq. (13).

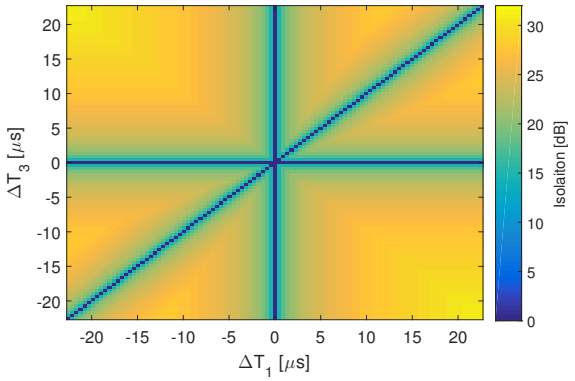


Fig. 4. Optimisation results for the waveform set 4. Isolation of the the entire set is shown as a function of optimisation parameters ΔT_1 and ΔT_3.

Doppler tolerance of each waveform depends on the longest LFM subchirp of the waveform. In general, if the time duration of the longest subchirp is increased, the filter mismatch due to Doppler shift will reduce. Doppler tolerance is not optimal as

TABLE I
WAVEFORM PARAMETERS AND ISOLATION FIGURES FOR THE PROPOSED WAVEFORM SETS.

	s_i	s_j	$\tau_{i,1}$ [µs]	$T_{i,1}$ [µs]	$f_{i,1}$ [MHz]	$B_{i,1}$ [MHz]	$\tau_{i,2}$ [µs]	$T_{i,2}$ [µs]	$f_{i,2}$ [MHz]	$B_{i,2}$ [MHz]	$\overline{I}_{i,j}$ [dB]	$\overline{M}_i$ [dB]	$\overline{P}_{i,j}$ [dB]	$\overline{I}_{set}$ [dB]
Set 1	s_1	s_2	-25.000	25.000	-50.0	50.0	0.000	25.000	0.0	50.0	37.44	-0.23	40.07	
	s_2	s_3	-25.000	25.000	50.0	-50.0	0.000	25.000	0.0	-50.0	32.18	-0.23	50.40	32.18
	s_3	s_1	-25.000	25.000	-50.0	100.0	0.000	25.000	50.0	-100.0	32.18	-7.19	50.40	
Set 2	s_1	s_2	-25.000	24.575	-50.0	25.0	-0.425	25.425	50.0	-75.0	31.36	-6.20	58.93	
	s_2	s_3	-25.000	24.575	-50.0	50.0	-0.425	25.425	50.0	-50.0	31.37	-6.11	59.72	31.36
	s_3	s_1	-25.000	24.575	-50.0	75.0	-0.425	25.425	50.0	-25.0	32.23	-6.07	55.52	
Set 3	s_1	s_2	-25.000	25.000	-50.0	50.0	0.000	25.000	0.0	50.0	32.53	-0.23	70.02	
	s_2	s_3	-25.000	25.000	-50.0	0.0	0.000	25.000	-50.0	100.0	29.17	-7.19	71.96	28.77
	s_3	s_1	-25.000	25.000	-50.0	87.0	0.000	25.000	37.0	13.0	28.77	-6.06	72.42	
Set 4	s_1	s_2	-25.000	47.500	-50.0	100.0	22.500	2.500	50.0	-100.0	31.12	-0.72	42.70	
	s_2	s_3	-25.000	25.000	-50.0	100.0	0.000	25.000	50.0	-100.0	31.12	-7.19	42.70	31.12
	s_3	s_1	-25.000	2.500	-50.0	100.0	-22.500	47.500	50.0	-100.0	35.24	-0.72	40.90	
Set 5	s_1	s_2	-25.000	47.500	-50.0	100.0	22.500	2.500	50.0	-100.0	32.01	-0.73	51.53	
	s_2	s_3	-25.000	25.000	-50.0	100.0	0.000	25.000	50.0	-100.0	32.01	-7.19	51.53	32.01
	s_3	s_1	-25.000	2.500	-50.0	100.0	-22.500	47.500	50.0	-100.0	35.25	-0.73	40.90	

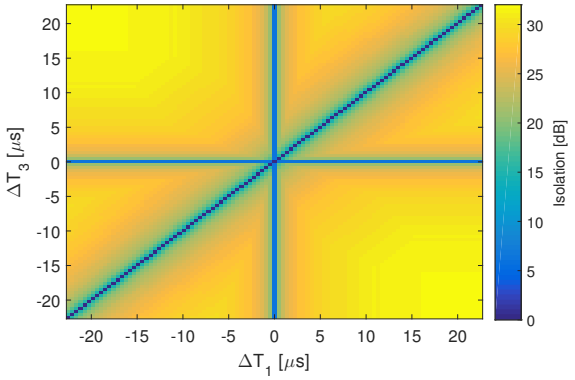


Fig. 5. Optimisation results for the waveform set 5. Isolation of the the entire set is shown as a function of optimisation parameters ΔT_1 and ΔT_3.

the filter mismatch for most waveforms decreases to $-6\,\mathrm{dB}$ but it still has an advantage over polyphase codes [14]. This can be observed in the third column of Fig. 1 that shows filter mismatch $M_i(f_D)$ for each set.

IV. CONCLUSION

In this paper, orthogonal properties of piecewise LFM waveforms were investigated. It was shown that increasing time-bandwidth product increases the isolation between the waveforms. The use of linear subchirps ensures that the waveforms show Doppler tolerant properties to a certain degree. Additionally, it was demonstrated that the isolation figures do not vary significantly when the bandwidth and time duration of a set of waveforms is fixed. The insights presented herein can be used to employ more complex optimisation techniques for waveform generation.

ACKNOWLEDGEMENT

The authors would like to express gratitude to the MCM-ITP programme and Thales Optronique for funding this research.

REFERENCES

[1] J. Li and P. Stoica, *MIMO Radar Signal Processing*. New Jersey, USA: John Wiley & Sons, 2009.
[2] J. Kantor and S. K. Davis, "Airborne GMTI Using MIMO Techniques," *2010 IEEE Radar Conference*, pp. 1344–1349, 2010.
[3] S. Liu, Z. Zhang, and W. Yu, "A Space-Time Coding Scheme With Time and Frequency Comb-Like Chirp Waveforms for MIMO-SAR," *IEEE Journal of Selected Topics in Signal Processing*, vol. 11, no. 2, pp. 391–403, 2017.
[4] L. L. Monte, T. A. Corigliano, B. Himed, and C. J. Baker, "Dynamic range considerations in code division multiple input multiple output radar," *IET Radar, Sonar & Navigation*, vol. 10, no. 8, pp. 1375–1383, 2016.
[5] L. Kocjancic, A. Balleri, and T. Merlet, "Multibeam radar based on linear frequency modulated waveform diversity," *IET Radar, Sonar Navigation*, vol. 12, no. 11, pp. 1320–1329, 2018.
[6] L. Kocjancic, A. Balleri, and T. Merlet, "Experiments of quasi-orthogonal linear frequency modulated waveforms for multibeam radar," in *2019 IEEE Radar Conference*, Boston, US, 2019.
[7] H. Li, Y. Zhao, Z. Cheng, and D. Feng, "OFDM chirp waveform diversity design with correlation interference suppression for MIMO radar," *IEEE Geoscience and Remote Sensing Letters*, vol. 14, no. 7, pp. 1032–1036, 2017.
[8] G. Chang, A. Liu, C. Yu, Y. Ji, Y. Wang, and J. Zhang, "Orthogonal Waveform With Multiple Diversities for MIMO Radar," *IEEE Sensors Journal*, vol. 1748, no. 3, pp. 1–1, 2018.
[9] L. Kocjancic, A. Balleri, and T. Merlet, "Study of the Frequency Slope Effect on the Chirp Waveform Orthogonality," in *International Conference on Radar Systems*, Belfast, UK, 2017.
[10] H. Shen and A. Papandreou-Suppappola, "Diversity and channel estimation using time-varying signals and time-frequency techniques," *IEEE Transactions on Signal Processing*, vol. 54, no. 9, pp. 3400–3413, 2006.
[11] W.-Q. Wang, "MIMO SAR Chirp Modulation Diversity Waveform Design," *IEEE Geoscience and Remote Sensing Letters*, vol. 11, no. 9, pp. 1644–1648, 2014.
[12] F. A. Qazi and A. T. Fam, "Doppler tolerant and detection capable polyphase code sets," *IEEE Transactions on Aerospace and Electronic Systems*, vol. 51, no. 2, pp. 1123–1135, apr 2015.
[13] Wang, Wen-Qin, "Large Time-Bandwidth Product MIMO Radar Waveform Design Based on Chirp Rate Diversity," *IEEE Sensors Journal*, vol. 15, no. 2, pp. 1027–1034, feb 2015.
[14] H. Deng, "Polyphase Code Design for Orthogonal Netted Radar Systems," *IEEE Transactions on Signal Processing*, vol. 52, no. 11, pp. 3126–3135, Nov 2004.



https://dspace.org/

Numerical characterisation of quasi-orthogonal piecewise linear frequency modulated waveforms

Kocjancic, Leon; Balleri, Alessio; Merlet, Thomas

2019-07-01
IEEE
https://doi.org/10.1109/SSPD.2019.8751653
Kocjancic L, Balleri A, Merlet T. Numerical characterisation of quasi-orthogonal piecewise linear frequency modulated waveforms. 2019 Sensor Signal Processing for Defence Conference (SSPD), Brighton, 9-10 May 2019

Downloaded from a DSpace repository. https://dspace.org/